12th International Symposium on Turbulence and Shear Flow Phenomena (TSFP12)
Osaka, Japan (Online), July 19–22, 2022

A SUB-GRID ACTIVITY SENSOR APPLIED TO MIXED MODELING IN LARGE EDDY SIMULATION

Josef Hasslberger
Institute of Applied Mathematics and Scientific Computing
Department of Aerospace Engineering, University of the Bundeswehr Munich
Werner-Heisenberg-Weg 39, 85577 Neubiberg, Germany
josef.hasslberger@unibw.de

SUB-GRID SCALE MODELING

Mixed models, i.e. a combination of functional and structural sub-grid scale (SGS) models, are among the most successful approaches for Large Eddy Simulation (LES). Compared to purely structural models, mixed models are especially superior in terms of stability. Chapelier *et al.* (2018) have recently demonstrated the potential of a sub-grid activity sensor to improve the performance of functional eddy viscosity models in regions with transitional flow features. Further, it has been shown by Hasslberger *et al.* (2021) how a sub-grid activity sensor can additionally be used to rectify the incorrect near-wall scaling of eddy viscosity base models like the standard Smagorinsky model without explicit wall damping. Accordingly, the idea here is to exploit the advantages of a sub-grid activity sensor in the context of mixed SGS modeling.

The coherent structure function, as required in the following analysis, is a useful quantity to characterize the structure of turbulent flows. It is defined as $F_{CS} = Q/E$, i.e. the second invariant of the grid-scale velocity gradient tensor

$$Q = (\overline{\Omega}_{ij}\overline{\Omega}_{ij} - \overline{S}_{ij}\overline{S}_{ij})/2 \tag{1}$$

being normalized by its magnitude

$$E = (\overline{\Omega}_{ij}\overline{\Omega}_{ij} + \overline{S}_{ij}\overline{S}_{ij})/2 \tag{2}$$

where $\overline{S}_{ij} = (\partial \overline{u}_i/\partial x_j + \partial \overline{u}_j/\partial x_i)/2$ is the grid-scale strain tensor and $\overline{\Omega}_{ij} = (\partial \overline{u}_i/\partial x_j - \partial \overline{u}_j/\partial x_i)/2$ is the grid-scale rotation tensor. Consequently, F_{CS} exhibits a definite lower and upper limit, i.e. $-1 \leq F_{CS} \leq +1$. The values -1 and $+1$ correspond to pure elongation/strain and pure rotation, respectively. It is important to note that the constituents of Q and E are related to fundamental quantities to describe turbulent flows, namely the dissipation of kinetic energy into heat per unit mass, $2\nu S_{ij}S_{ij}$, and enstrophy, $\Omega_{ij}\Omega_{ij}$.

The best-known functional SGS model is the standard Smagorinsky model (Smagorinsky, 1963) which calculates the deviatoric part $\tau_{ij}^{dev} = \tau_{ij} - \frac{1}{3}\tau_{kk}\delta_{ij}$ of the SGS stress tensor for incompressible flows $\tau_{ij} = \overline{u_i u_j} - \overline{u}_i\overline{u}_j$ as

$$\tau_{ij}^{EV} = -2\,C_{Smago}^2\Delta^2\sqrt{2\overline{S}_{kl}\overline{S}_{kl}}\,\overline{S}_{ij} = -2\nu_t\overline{S}_{ij} \tag{3}$$

where Δ is the grid size (i.e. the implicit filter width), ν_t is the eddy viscosity (EV) and $C_{Smago} = 0.17$ is the theoretical value of the Smagorinsky constant.

In contrast to functional eddy viscosity models, structural models aim to reproduce the structure of the SGS stress tensor itself and, among those, the Bardina/Liu model (Bardina, 1983; Liu *et al.*, 1994)

$$\tau_{ij}^{SS} = \widehat{\overline{u}_i\overline{u}_j} - \widehat{\overline{u}}_i\widehat{\overline{u}}_j \tag{4}$$

is based on the scale similarity (SS) principle, where $\widehat{(\cdot)}$ represents a suitably defined explicit test filter. In this work, the explicit test filter for any field quantity $\phi_{i,j,k}$ at the discrete location given by the index triple (i,j,k) is implemented according to Anderson & Domaradzki (2012):

$$\widehat{\phi}_{i,j,k} = \sum_{l=-1}^{+1}\sum_{m=-1}^{+1}\sum_{n=-1}^{+1} b_l \cdot b_m \cdot b_n \cdot \phi_{i+l,j+m,k+n} \tag{5}$$

This three-dimensional filter is the product of the convolution of three one-dimensional filters with coefficients $(b_{-1}, b_0, b_{+1}) = (c^{fil}, 1-2c^{fil}, c^{fil})$ where $c^{fil} = 1/12$.

The following blending scheme is based on the below observation that structural models of the scale similarity (SS) type perform the best for moderate under-resolution of the flow, whereas the concept of eddy viscosity (EV) becomes increasingly valid the lower the relative resolution is. Hence, the idea is to retain the superior alignment properties of SS models in those regions where an extrapolation based on the smallest resolved scales (which are also strongly affected by numerical errors) is still properly working, and to blend in a more robust EV model where physically plausible. Using a local sub-grid activity sensor Θ, the blending scheme reads

$$\tau_{ij}^{mixed,sensor} = \tau_{ij}^{EV}\,\Theta + \tau_{ij}^{SS}(1-\Theta) \tag{6}$$

where τ_{ij}^{EV} and τ_{ij}^{SS} represent any kind of eddy viscosity and scale similarity type model, respectively. The lower the relative resolution, the higher the sub-grid activity Θ and the higher (lower) the EV (SS) contribution is. This is also consistent from a physical point of view, because "randomly" fluctuating incoherent turbulence acts like diffusive motion – agreeing with the way eddy viscosity is reflected in the diffusive term of the filtered Navier-Stokes equations.

The bounded sensor function Θ is constructed as

$$\Theta = \begin{cases} 1 & \sigma < \sigma_{eq} \\ \frac{1}{2}\left(1+\sin\left(\pi\frac{\sigma_{eq}-2\sigma+1}{2(1-\sigma_{eq})}\right)\right) & \text{if } \sigma \in [\sigma_{eq},1] \\ 0 & \sigma > 1 \end{cases} \quad (7)$$

such that a smooth transition between well-resolved ($\sigma > 1$) and insufficiently-resolved ($\sigma < \sigma_{eq}$) regions is obtained. Although Eq. 7 is the same as in (Chapelier *et al.*, 2018), σ is calculated in a different manner. Rather than using enstrophy only, $\sigma = \widehat{E}/E$ accounts for both dissipation and enstrophy. Comparison of the implicitly grid-filtered value E and the explicitly test-filtered value $\widehat{E}$ allows to estimate the local subgrid activity. At the same time, the intensity-preserving ($E \approx$ const.; $\widehat{E} \approx$ const.) natural exchange between dissipation and enstrophy in turbulent flows remains undetected by the sensor. According to the definition of E, Eq. 2, fluctuations in strain- and rotation-dominated flow regions can be equally well reflected by the sensor. This is demonstrated in Fig. 1 which depicts conditionally averaged values of the sub-grid activity Θ in homogeneous isotropic turbulence (details on this a-priori analysis are provided subsequently). The original sensor formulation based on enstrophy only (left panel of Fig. 1) is obviously unable to detect sub-grid activity in strain-dominated flow regions. Independent of the implicit filter width in LES, strain-dominated flow regions are even more probable than rotation-dominated flow regions in turbulent flows as shown by the probability density function (PDF) of the coherent structure function F_{CS} in Fig. 2. Agreeing with expectations, Fig. 1 demonstrates increasing levels of sub-grid activity Θ for increasing under-resolution of the flow as specified by Δ/Δ_{DNS}.

The calculation of the equilibrium value σ_{eq} is identical to Chapelier *et al.* (2018) since dissipation and enstrophy are obeying the same spectral scaling. Both spectra are proportional to $\kappa^2 e(\kappa)$ with wavenumber κ and energy spectrum $e(\kappa)$. Their peak is located at high wavenumbers (small scales), hence also the naming as a sub-grid activity sensor. On average, $\widehat{E} < E$ in the inertial sub-range. The equilibrium value is given by

$$\sigma_{eq} = \left(\frac{\widehat{\Delta}}{\Delta}\right)^{-4/3} = \left(\sqrt{24\, c^{fil}}\right)^{-4/3} \quad (8)$$

where the ratio of explicit-to-implicit filter width $\widehat{\Delta}/\Delta$ has been further reduced to the filter coefficients following Lund (1997). For the explicit test filter applied here, $c^{fil} = 1/12$ yields $\sigma_{eq} = 2^{-2/3} \approx 0.63$.

A-PRIORI ANALYSIS

To justify the above mixed modeling idea, the SGS energy transfer behavior of the separate functional and structural base models is analyzed by means of an a-priori analysis. The comparably well-defined state of homogeneous isotropic turbulence (closely resembled by the final stage of the Taylor-Green vortex, cf. $t = 25$ in Fig. 4) is chosen for this purpose. The Direct Numerical Simulation (DNS) database, uniformly discretized by 512^3 grid points, has been explicitly filtered using a Gaussian filter kernel for varying normalized filter width Δ/Δ_{DNS}. It is particularly instructive to analyze the performance conditional on the coherent structure function F_{CS} due to the intricate dissipation-enstrophy interplay in turbulent flows. Also, the SGS energy transfer $\varepsilon = \tau_{ij}\overline{S}_{ij}$ can be decomposed into forward scatter $\varepsilon^- = 0.5(\varepsilon - |\varepsilon|)$ and backward scatter $\varepsilon^+ = 0.5(\varepsilon + |\varepsilon|)$. For consistency, only the deviatoric part of SGS stress is considered for the EV model, although the discrepancy between $\tau_{ij}^{dev} = \tau_{ij} - \frac{1}{3}\tau_{kk}\delta_{ij}$ and τ_{ij} is small here.

Figure 3 shows that for moderate filter width ($\Delta/\Delta_{DNS} = 9$), the Bardina/Liu model clearly outperforms the Smagorinsky model, because the latter is overly dissipative. For large filter width ($\Delta/\Delta_{DNS} = 33$), both types of models are in good agreement with the reference data. Under these conditions, the SGS energy transfer, on average, is almost linearly increasing from rotation- to strain-dominated regions and this can be represented also by the Smagorinsky model. Although not explicitly shown here, tendencies with respect to Reynolds number variation are expected to be similar than for filter width variation. It cannot be seen from this a-priori analysis but it is known that structural models tend to become unstable under high filter width/Reynolds number conditions which motivates the mixed model. It is worth noting that the SS model is able to represent backward scatter in contrast to the EV model. Backward scatter is not unphysical but is discussed as a potential source of instability for structural models in the literature (Kobayashi, 2018; Klein *et al.*, 2020).

A-POSTERIORI ANALYSIS

The open-source code PARIS[1] (Aniszewski *et al.*, 2021) has been employed to solve the unsteady incompressible Navier-Stokes equations. It uses a second-order Runge-Kutta technique for time integration and spatial discretization is realized by the finite-volume approach on a regular, cubic staggered grid with second-order centered difference schemes. In the framework of the projection method, the pressure field is calculated by a multi-grid Poisson solver provided by the HYPRE library.

The Taylor-Green vortex (Brachet *et al.*, 1983) is a challenging test case for laminar-turbulent transition and this configuration consists of a cube with side length 2π and periodic boundaries in all directions. The velocity field is initialized as

$$u(x,y,z) = \cos(x)\sin(y)\sin(z) \quad (9)$$
$$v(x,y,z) = -\sin(x)\cos(y)\sin(z) \quad (10)$$
$$w(x,y,z) = 0 \quad (11)$$

Referring to the initial state, the Reynolds number is 1600 and the density is assumed to be constant. Two different resolutions have been investigated, i.e. the benchmark DNS and a much coarser 32^3 grid for all a-posteriori LES runs. Hence, the computational costs are considerably different. The non-dimensional simulation time ranges from $t = 0$ to $t = 25$ and the corresponding development of the flow in the DNS is shown in Fig. 4. Through vortex breakdown, the flow evolves from a quasi-laminar initial condition to fairly homogeneous fully developed turbulence at the final stage considered.

Figure 5 shows the temporal evolution of the mean kinetic energy and its dissipation rate for the no-model LES, the Smagorinsky model, the Bardina/Liu model and the sensor-based mixed model. Both the filtered and unfiltered DNS results are included as references. As expected, the EV model is overly dissipative during the quasi-laminar initial stage. The SS model underpredicts the peak dissipation and shows first

[1] http://www.ida.upmc.fr/∼zaleski/paris/

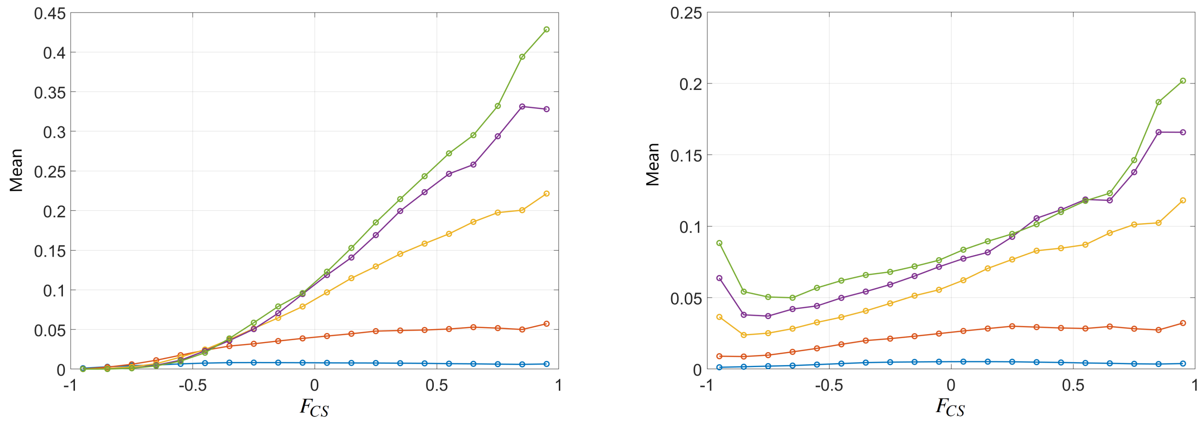

Figure 1. Homogeneous isotropic turbulence: Means of the sub-grid activity sensor Θ conditional on the coherent structure function F_{CS}, where -1 and $+1$ correspond to pure strain and pure rotation, respectively. Results are shown for filter width $\Delta/\Delta_{DNS} = 3$ (blue), 5 (red), 9 (yellow), 13 (purple), 17 (green). Original formulation based on enstrophy on the left, present formulation based on enstrophy and dissipation on the right.

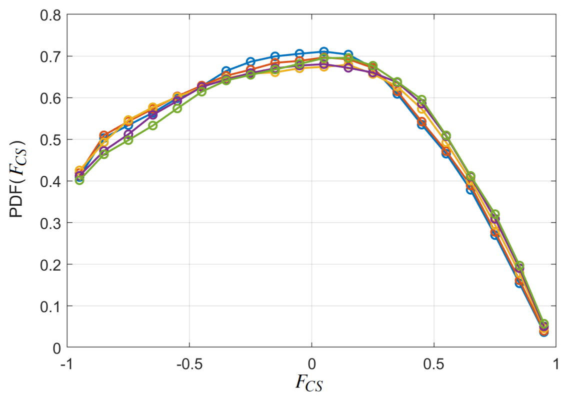

Figure 2. Homogeneous isotropic turbulence: Probability density function (PDF) of the coherent structure function F_{CS}, where -1 and $+1$ correspond to pure strain and pure rotation, respectively. Results are shown for filter width $\Delta/\Delta_{DNS} = 3$ (blue), 5 (red), 9 (yellow), 13 (purple), 17 (green).

signs of instability, i.e. oscillations of the dissipation curve, during the high-dissipation phase around $5 < t < 15$. In contrast, the sensor-based mixed model correctly reduces to the filtered DNS in the initial stage, improves the peak dissipation and also appears to be more robust during the high-dissipation phase. A clear improvement compared to the no-model LES can be observed as well.

The difference between the original sensor by Chapelier *et al.* (2018) based on enstrophy ($\Omega_{ij}\Omega_{ij}$) and the present modified sensor based on the sum of enstrophy and dissipation ($E = (\overline{\Omega}_{ij}\overline{\Omega}_{ij} + \overline{S}_{ij}\overline{S}_{ij})/2$) can be discerned from Fig. 6. Although the overall results are quite similar, the mixed model using the newly proposed sensor is somewhat less oscillatory, which can be seen especially during the high-dissipation phase around $5 < t < 15$. Only the modified sensor variant based on E is thus used in the following.

A viable alternative for the structural part of the mixed model is the gradient model by Clark *et al.* (1979):

$$\tau_{ij}^{SS} = \frac{\Delta^2}{12} \frac{\partial \overline{u}_i}{\partial x_k} \frac{\partial \overline{u}_j}{\partial x_k} \tag{12}$$

Again, the sensor-based mixed model leads to a clear improvement over the separate structural model as can be seen in Fig. 7. As expected, the curves start to diverge considerably when the level of under-resolution becomes significant at $t \approx 4$. In this case, the improvement through the sensor-based regularization is even more obvious than with the Bardina/Liu model combination (Fig. 5).

CONCLUSIONS AND OUTLOOK

A strategy for mixed modeling in LES is proposed by means of a sub-grid activity sensor based blending between the functional and structural base models. This mixed model outperforms the separate base models (here: Bardina/Liu or Clark and Smagorinsky) for the Taylor-Green vortex test case and is oscillation-free without additional regularization like averaging (in homogeneous direction), relaxation in time or clipping (of backscatter). It is worth noting that the overall model is also parameter-free, apart from the choice of the test filter.

Since not discussed here, future work will focus on the wall treatment for the proposed mixed model. This can be achieved either by replacing the current base models with models that already incorporate the correct wall scaling, e.g. (Nicoud *et al.*, 2011), or by using a wall-scaling sensor, e.g. (Hasslberger *et al.*, 2021), in addition to the non-wall scaling sensor Θ for blending. Note that also the structural models by

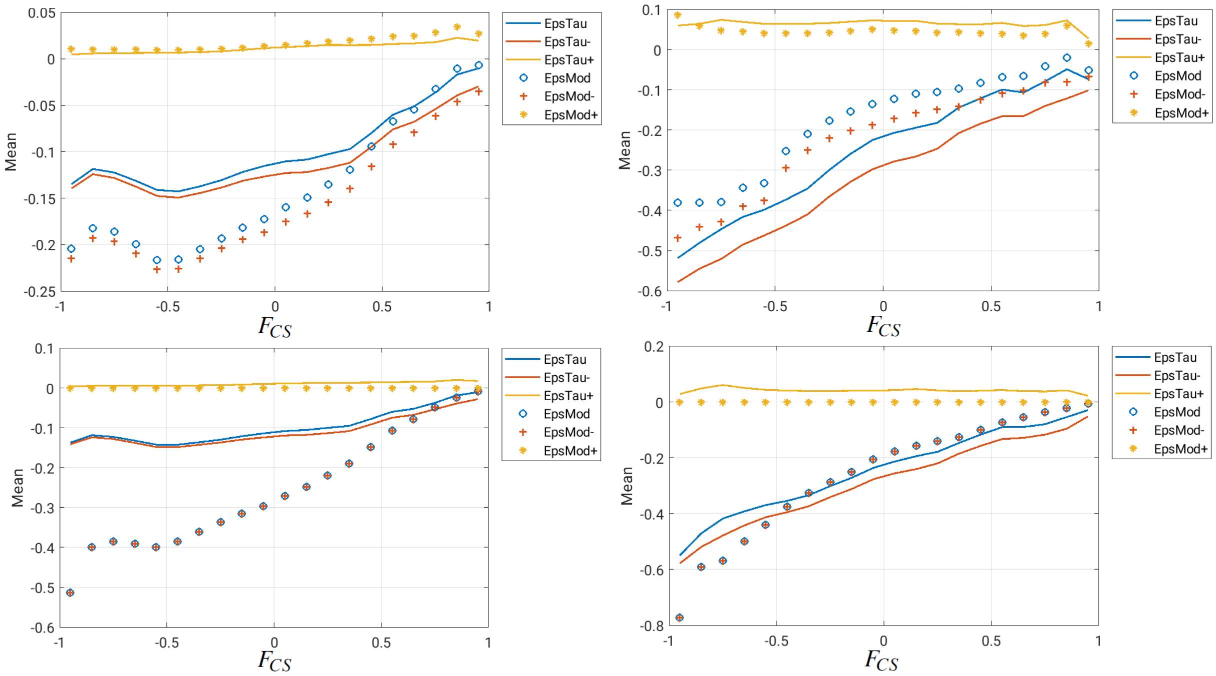

Figure 3. Homogeneous isotropic turbulence: Means of the "true" SGS energy transfer $\tau_{ij}^{DNS}\overline{S}_{ij}$ (EpsTau, continuous lines) and model energy transfer $\tau_{ij}^{model}\overline{S}_{ij}$ (EpsMod, marker symbols) conditional on the coherent structure function F_{CS}. Eps- and Eps+ indicate forward scatter ε^- and backward scatter ε^+. Results are shown for the Bardina/Liu model (top row) and Smagorinsky model (bottom row) for moderate, i.e. $\Delta/\Delta_{DNS} = 9$ (left), and large filter width, i.e. $\Delta/\Delta_{DNS} = 33$ (right), respectively. Note the different scales of the ordinate axes.

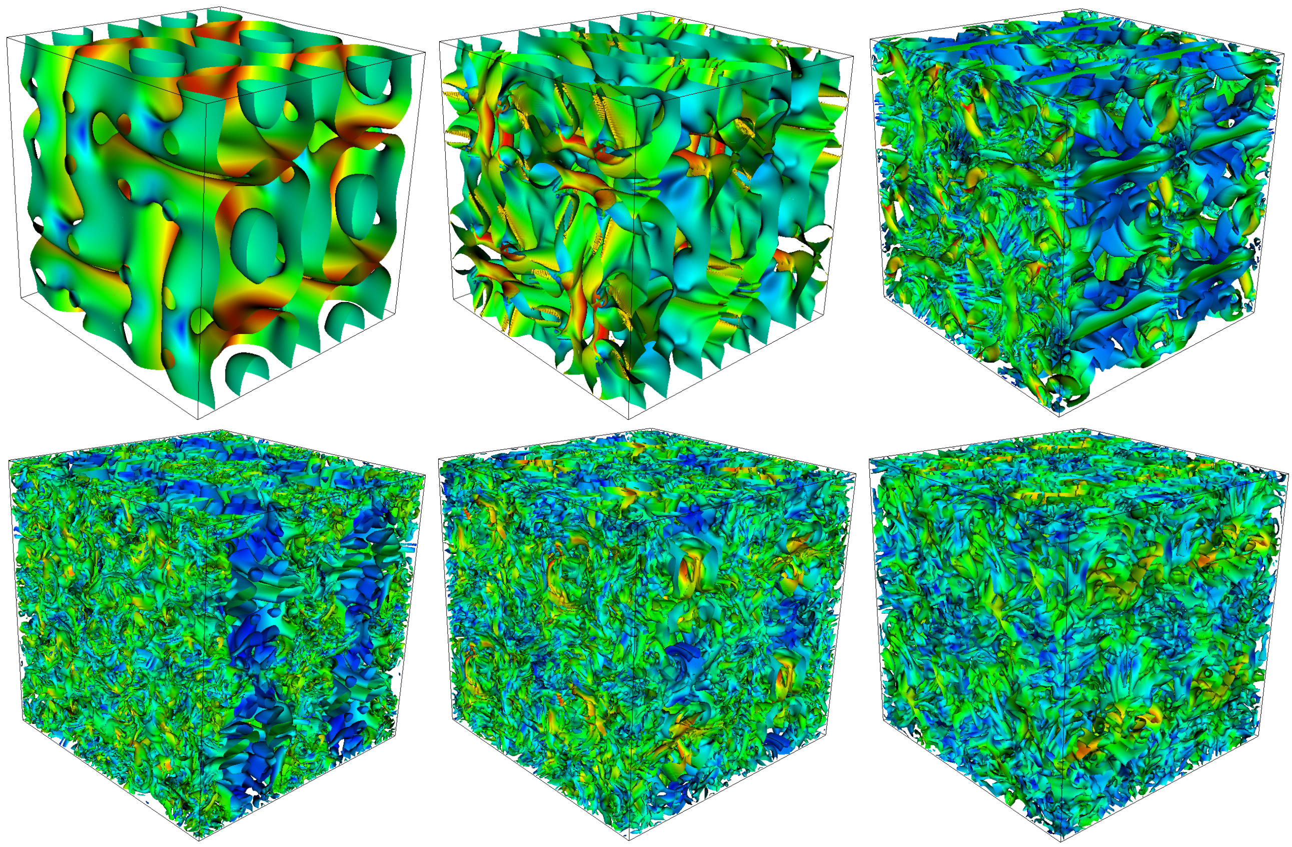

Figure 4. Stages of the Taylor-Green vortex as seen in the reference DNS: Instantaneous views of $F_{CS} = 0$ iso-contours coloured by the velocity magnitude at simulation times t = 2.5, 5, 7.5, 10, 15, 25.

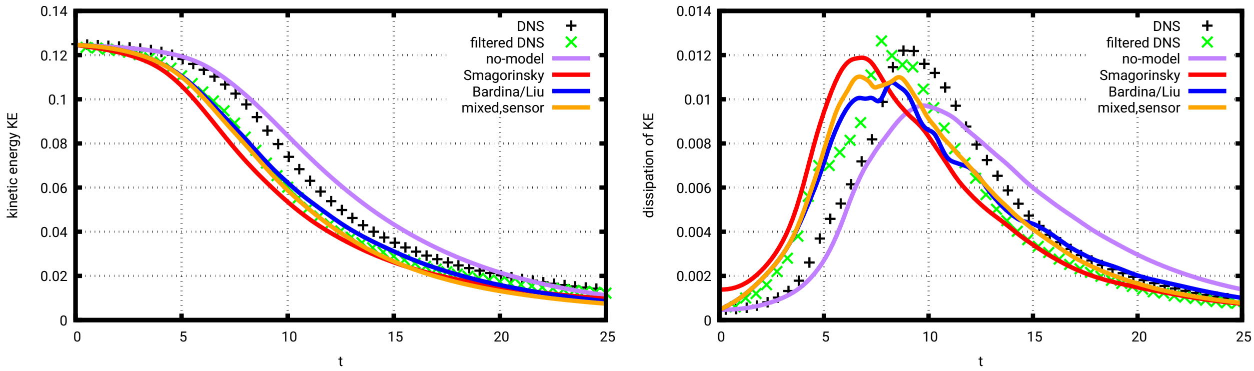

Figure 5. Taylor-Green vortex: Volume-averaged kinetic energy (left) and its dissipation rate (right) versus non-dimensional time for the reference DNS, the no-model LES, the Smagorinsky model, the Bardina/Liu model and the sensor-based mixed model.

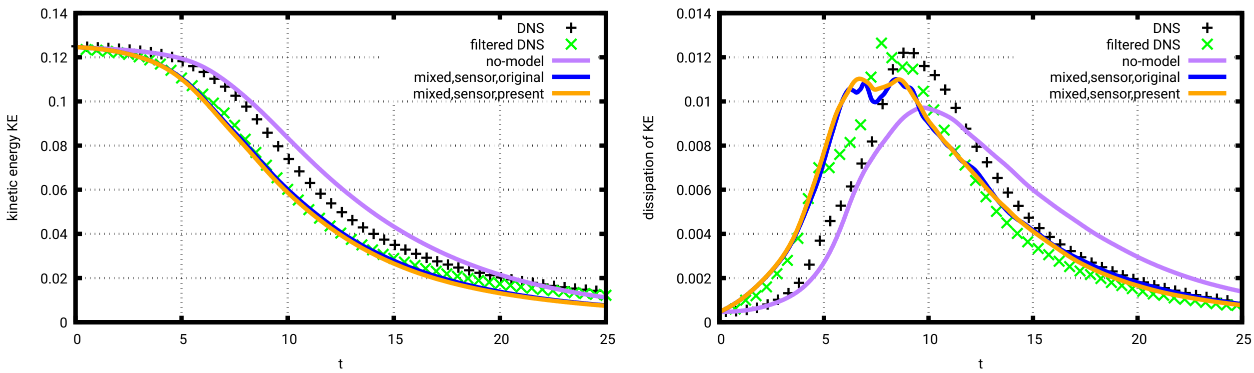

Figure 6. Taylor-Green vortex: Volume-averaged kinetic energy (left) and its dissipation rate (right) versus non-dimensional time for the reference DNS, the no-model LES, the mixed model using the original sensor based on enstrophy only and the mixed model using the newly proposed sensor based on the sum of enstrophy and dissipation.

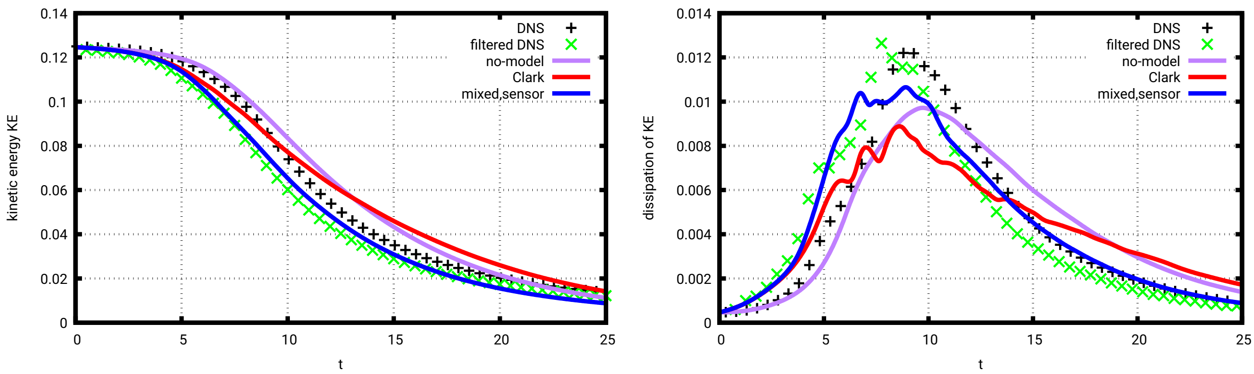

Figure 7. Taylor-Green vortex: Volume-averaged kinetic energy (left) and its dissipation rate (right) versus non-dimensional time for the reference DNS, the no-model LES, the separate model by Clark et al. and the sensor-based mixed model using the structural model by Clark et al. instead of Bardina/Liu et al.

Bardina/Liu et al. as well as Clark et al. suffer from incorrect near-wall scaling (Silvis *et al.*, 2017).

REFERENCES

Anderson, BW & Domaradzki, JA 2012 A subgrid-scale model for large-eddy simulation based on the physics of interscale energy transfer in turbulence. *Physics of Fluids* **24** (6), 065104.

Aniszewski, W, Arrufat, T, Crialesi-Esposito, M, Dabiri, S, Fuster, D, Ling, Y, Lu, J, Malan, L, Pal, S, Scardovelli, R *et al.* 2021 Parallel, robust, interface simulator (PARIS). *Computer Physics Communications* **263**, 107849.

Bardina, J 1983 Improved turbulence models based on large eddy simulation of homogeneous, incompressible, turbulent flows. PhD thesis, Stanford University.

Brachet, ME, Meiron, DI, Orszag, SA, Nickel, BG, Morf, RH & Frisch, U 1983 Small-scale structure of the Taylor–Green vortex. *Journal of Fluid Mechanics* **130**, 411–452.

Chapelier, J-B, Wasistho, B & Scalo, C 2018 A coherent vorticity preserving eddy-viscosity correction for large-eddy simulation. *Journal of Computational Physics* **359**, 164–182.

Clark, RA, Ferziger, JH & Reynolds, WC 1979 Evaluation of subgrid-scale models using an accurately simulated turbulent flow. *Journal of Fluid Mechanics* **91** (1), 1–16.

Hasslberger, J, Engelmann, L, Kempf, A & Klein, M 2021 Robust dynamic adaptation of the Smagorinsky model based on a sub-grid activity sensor. *Physics of Fluids* **33** (1), 015117.

Klein, M, Ketterl, S, Engelmann, L, Kempf, A & Kobayashi, H 2020 Regularized, parameter free scale similarity type models for large eddy simulation. *International Journal of Heat and Fluid Flow* **81**, 108496.

Kobayashi, H 2018 Improvement of the sgs model by using a scale-similarity model based on the analysis of sgs force and sgs energy transfer. *International Journal of Heat and Fluid Flow* **72**, 329–336.

Liu, S, Meneveau, C & Katz, J 1994 On the properties of similarity subgrid-scale models as deduced from measurements in a turbulent jet. *Journal of Fluid Mechanics* **275**, 83–119.

Lund, TS 1997 On the use of discrete filters for large eddy simulation. *Annual Research Briefs* pp. 83–95.

Nicoud, F, Toda, HB, Cabrit, O, Bose, S & Lee, J 2011 Using singular values to build a subgrid-scale model for large eddy simulations. *Physics of Fluids* **23** (8), 085106.

Silvis, MH, Remmerswaal, RA & Verstappen, R 2017 Physical consistency of subgrid-scale models for large-eddy simulation of incompressible turbulent flows. *Physics of Fluids* **29** (1), 015105.

Smagorinsky, J 1963 General circulation experiments with the primitive equations: I. the basic experiment. *Monthly Weather Review* **91** (3), 99–164.